



NRL/MR/7681--19-9907

Modeling Solar Irradiance Variability and the Ionospheric Response to Solar Flares

JEFFREY W. REEP
HARRY P. WARREN
NICHOLAS A. CRUMP
KALMAN J. KNIZHNIK
STEPHEN J. BRADSHAW

*Solar and Heliospheric Physics Branch
Space Science Division*

December 17, 2019

DISTRIBUTION STATEMENT A: Approved for public release, distribution is unlimited.

REPORT DOCUMENTATION PAGE

Form Approved
OMB No. 0704-0188

Public reporting burden for this collection of information is estimated to average 1 hour per response, including the time for reviewing instructions, searching existing data sources, gathering and maintaining the data needed, and completing and reviewing this collection of information. Send comments regarding this burden estimate or any other aspect of this collection of information, including suggestions for reducing this burden to Department of Defense, Washington Headquarters Services, Directorate for Information Operations and Reports (0704-0188), 1215 Jefferson Davis Highway, Suite 1204, Arlington, VA 22202-4302. Respondents should be aware that notwithstanding any other provision of law, no person shall be subject to any penalty for failing to comply with a collection of information if it does not display a currently valid OMB control number. **PLEASE DO NOT RETURN YOUR FORM TO THE ABOVE ADDRESS.**

1. REPORT DATE (DD-MM-YYYY) 17-12-2019			2. REPORT TYPE NRL Memorandum Report		3. DATES COVERED (From - To) April 30, 2018 – April 30, 2019	
4. TITLE AND SUBTITLE Modeling Solar Irradiance Variability and the Ionospheric Response to Solar Flares					5a. CONTRACT NUMBER	
					5b. GRANT NUMBER	
					5c. PROGRAM ELEMENT NUMBER NISE	
6. AUTHOR(S) Jeffrey W. Reep, Harry P. Warren, Nicholas A. Crump, Kalman J. Knizhnik, and Stephen J. Bradshaw					5d. PROJECT NUMBER 76-N2P2-08	
					5e. TASK NUMBER	
					5f. WORK UNIT NUMBER N2P2	
7. PERFORMING ORGANIZATION NAME(S) AND ADDRESS(ES) Naval Research Laboratory 4555 Overlook Avenue, SW Washington, DC 20375-5320					8. PERFORMING ORGANIZATION REPORT NUMBER NRL/MR/7681--19-9907	
9. SPONSORING / MONITORING AGENCY NAME(S) AND ADDRESS(ES) Naval Research Laboratory 4555 Overlook Avenue, SW Washington, DC 20375-5320					10. SPONSOR / MONITOR'S ACRONYM(S) NRL-NISE	
					11. SPONSOR / MONITOR'S REPORT NUMBER(S)	
12. DISTRIBUTION / AVAILABILITY STATEMENT DISTRIBUTION STATEMENT A: Approved for public release distribution is unlimited.						
13. SUPPLEMENTARY NOTES						
14. ABSTRACT We developed a model to synthesize irradiance from a detailed hydrodynamic model of a solar flare. The model was developed to accurately calculate the details of the solar chromosphere, which is characterized by non-local thermodynamic equilibrium, necessitating a radiative transfer calculation. A method to solve this efficiently was implemented, tested against other models, and validated against observations of the chromosphere with data taken by NASA's IRIS satellite. We developed a multi-threaded model of a solar flare, accounting for the time-varying geometry, large number of loop structures, and time varying energy release. The parameters of this model were derived using data from NOAA's GOES satellite to determine heating rates and volumes for flares. Using this global model, we synthesized X-ray spectra that are then validated against an X-ray spectrometer for a set of five observed flares. These synthetic spectra are being developed for delivery to ionospheric general circulation models to calculate the impact of extreme flares on the Earth.						
15. SUBJECT TERMS Solar flares Irradiance Hydrodynamic modeling						
16. SECURITY CLASSIFICATION OF:			17. LIMITATION OF ABSTRACT	18. NUMBER OF PAGES	19a. NAME OF RESPONSIBLE PERSON	
a. REPORT	b. ABSTRACT	c. THIS PAGE			Jeffrey W. Reep	
Unclassified	Unclassified	Unclassified	Unclassified	19	19b. TELEPHONE NUMBER (include area code) (202) 767-2023	
Unlimited	Unlimited	Unlimited	Unlimited			

This page intentionally left blank.

CONTENTS

1. INTRODUCTION	1
2. OBSERVATIONS OF SOLAR FLARE PROPERTIES	2
2.1 Flare Size.....	2
2.2 Flare Duration.....	3
3. EFFICIENT MODELING OF THE SOLAR CHROMOSPHERE IN HYDRODYNAMIC SIMULATIONS	4
3.1 Hydrodynamic Simulations	5
3.2 Multithreaded Synthetic Light Curves	6
4. CONSTRUCTING A GLOBAL MODEL OF A SOLAR FLARE	7
4.1 Global Flaring Model – 2016 July 23 M5.0 Flare	8
4.2 Extrapolating the Global Flare Model.....	10
5. CONCLUSIONS	12
REFERENCES.....	14

This page intentionally left blank.

EXECUTIVE SUMMARY

This report presents research conducted by Reep et al. under his Karles Fellowship tenure at NRL, much of which is on-going. Solar irradiance variability has a direct impact upon the Earth's ionosphere-thermosphere system, and therefore understanding the causes of and changes in that variability are critical. Importantly, changes due to large flares can impact Navy communication systems, specifically HF and VHF radio systems and radar. The ultimate goal of this work is to better understand the energy release processes in solar flares to predict their impact upon the ionosphere, and therefore how communication systems will be affected. This work therefore addresses the goals of the DoD Space S&T Strategic Plan.

We have developed a model to synthesize irradiance from a detailed hydrodynamic model of a solar flare. The model has been developed to accurately calculate the details of the solar chromosphere, which is characterized by non-local thermodynamic equilibrium, necessitating a radiative transfer calculation. A method to solve this efficiently has been implemented, tested against other models, and validated against observations of the chromosphere with data taken by NASA's IRIS satellite. We have then developed a multi-threaded model of a solar flare, accounting for the time-varying geometry, large number of loop structures, and time varying energy release. The parameters of this model are derived using data from NOAA's GOES satellite, to determine heating rates and volumes for flares. Using this global model, we have synthesized X-ray spectra that are then validated against an X-ray spectrometer for a set of five observed flares. These synthetic spectra are being developed for delivery to ionospheric general circulation models to calculate the impact of extreme flares on the Earth.

This page intentionally left blank.

MODELING SOLAR IRRADIANCE VARIABILITY AND THE IONOSPHERIC RESPONSE TO SOLAR FLARES

1. INTRODUCTION

The impact of solar irradiance on the Earth's ionosphere-thermosphere-mesosphere system is critical for prediction of the impact upon radio communication systems. In solar flares, the irradiance at all wavelengths increases dramatically, and the X-ray irradiance in particular can cause drastic changes in the number density of electrons in the ionosphere. The specific altitudes that are affected depend on the intensity of the X-rays at specific wavelengths emitted by the flares. An accurate model of flares is key to prediction of the impact of flares upon the ionosphere, therefore, to determine how communication systems will be affected. Furthermore, extreme flares like the Carrington event (Carrington 1859) have not been observed with modern instrumentation, so a physical model is crucial to model these events. It is the goal of this work to not only predict the parameters of such an extreme event, but to understand how the Earth and radio systems could be affected.

Solar flares are caused by a magnetic reconnection event in the solar atmosphere, wherein energy stored in the magnetic fields are released as the field lines reconnect into a new geometry. This energy release causes the acceleration of particles (Holman et al. 2011), the generation of magnetohydrodynamic (MHD) waves (Tarr 2017), and *in situ* thermal heating (Cargill & Priest 1983). Each of these processes then transports energy across the solar atmosphere, from the solar corona down to the chromosphere, which is sharply heated, causing an explosion of plasma back into the corona (termed chromospheric evaporation, Hirayama 1974). The heating of the chromosphere produces brightenings from the extreme ultraviolet (EUV) through optical wavelengths, while the coronal plasma emits primarily in the EUV and soft X-rays (SXR), see e.g. Fletcher et al. (2011).

There are many outstanding issues in understanding solar flares and improving our models of them. First, the reconnection event creates a series of magnetic coronal loops that are heated in succession, referred to as a flare arcade (Sheeley et al. 2004). While many of the properties of the totality of a flare can be measured, the properties of individual loops are difficult if not impossible to measure with current instrumentation. A viable flare model must account for this, and properly treat each successive loop (Reep et al. 2016). Second, the chromosphere is optically thick at many wavelengths, and not in local thermodynamic equilibrium, which means that the full radiative transfer equation must be solved to accurately model it (Carlsson & Stein 2002). Third, the heating of flares is stochastic: there exists no method to predict accurately the properties of a flare, and many properties are not well understood. Finally, the accurate synthesis of spectral emissions or irradiance (done in post-processing) requires detailed atomic physics, accurate knowledge of the chemical abundances in the flares, and in general requires a radiative transfer calculation as well (Reep et al. 2019a).

In this report, we describe important steps that we have taken to measure distributions of flare properties, to create an accurate model of the flaring chromosphere in hydrodynamic simulations, to construct a global flaring model for any specified flare, and to calculate the irradiance from that

modeling effort. We have developed a method to scale the heating rates of smaller observed flares to large events expected to be at the limit of the Sun’s capability.

2. OBSERVATIONS OF SOLAR FLARE PROPERTIES

In order to create accurate models of solar flares to predict their irradiance, we must understand their basic properties and the distributions of those properties. Solar flares are routinely measured by the X-ray Ray Sensors (XRS) onboard the Geostationary Orbital Environmental Satellites (GOES) operated by NOAA. This series of satellites continuously monitors solar activity in two X-ray passbands: 0.1 – 0.8 nm (1.5–12 keV) and 0.05 – 0.4 nm (3–24 keV). Solar flares will produce noticeable brightenings above background levels in these channels, and in fact are classified according to their brightness in the 0.1–0.8 nm channel. X-class flares are defined to have flux levels exceeding 10^{-4} W m^{-2} , while M, C, B, and A class flares have brightness in decreasing decades (10^{-5} , 10^{-6} , 10^{-7} , 10^{-8} W m^{-2} , respectively).

From GOES XRS observations, we can determine the brightness (or class) of the flares, the durations of the flares, and through measuring ratios of the two channels their temperatures and emission measures (EMs, essentially a measure of the amount of plasma in the flare volume). A recent statistical study (Kazachenko et al. 2017) produced a database of flare geometrical properties using data from the Atmospheric Imaging Assembly (AIA) onboard the Solar Dynamics Observatory (SDO), including their ribbon areas, the size of the active regions in which they occur, and the total magnetic reconnection flux of the flares. We have combined this data set with observations made by GOES to examine distributions and trends in the properties of flares (Reep & Knizhnik 2019).

2.1 Flare Size

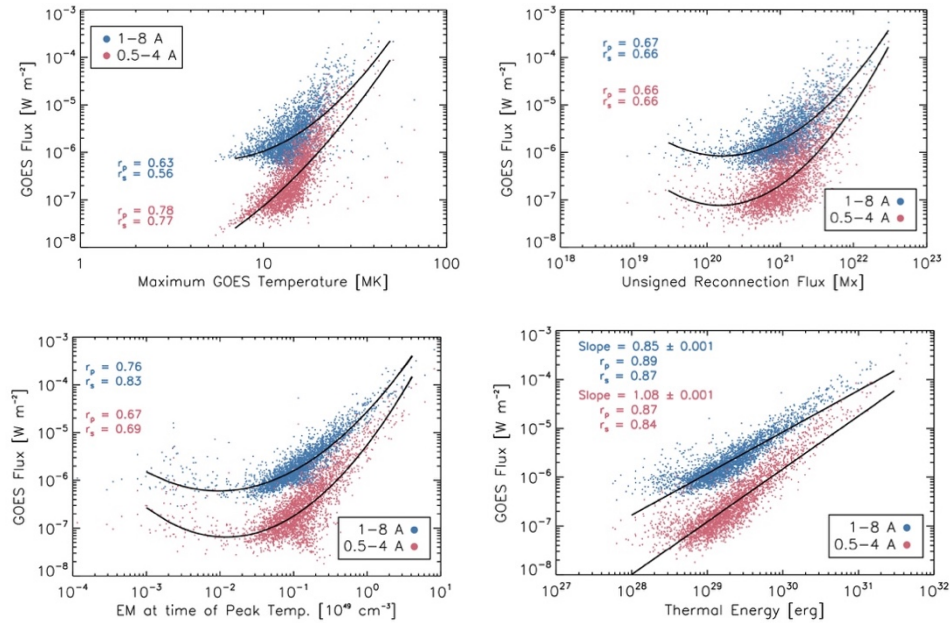


Fig. 1 — A summary of correlations between flare size (class) and the maximum temperature of the flare (top left), the magnetic reconnection flux (top right), the maximum emission measure (bottom left), and the total energy release (bottom right).

The intensity of the flare measured by GOES 0.1–0.8 nm determines the class or size of the flare. Flares are known to occur on a power law distribution in their total energy release (Hudson 1991), with an approximate power-law index of -2 , such that X-class flares are 100 times less likely to occur than M-class flares and so forth. Not surprisingly, the size of a flare is well correlated with many of its properties: the temperature, EM, magnetic reconnection flux, and total thermal energy release, which we show in Figure 1.

At the top left of Figure 1, we show the connection between the peak temperature and the size of the flare, which are weakly but positively correlated. That is, the temperature increases in larger flares, although not drastically. At the top right, we show the connection between the size of the flare and the amount of magnetic flux from the reconnection event (see also Kazachenko et al 2017). Not surprisingly, the more magnetic flux that is reconnected, the larger the flare is. At bottom left, we show that the EM at the time of the peak temperature is also strongly correlated with the GOES flux, which is unsurprising since it directly determines the strength of the emission. Finally, on the bottom right, we show that there is a direct and approximately linear correlation between the size of the flare and the total amount of energy released. The largest flares observed tend to release energy up to about 10^{32} erg, perhaps reaching 10^{33} erg in extreme events.

2.2 Flare Duration

The duration of a flare can be measured with the full-width-at-half-maximum (FWHM) in the two GOES XRS channels. Using these two channels, it can be shown that the durations are consistent with log-normal distributions, with median values of around 11 minutes in the low energy channel and 6 minutes in the high energy channel (Figure 2). Using a Kolmogorov-Smirnov test, we have found that the distribution in each passband is consistent with log-normal, and further that if the distributions are divided by the flare class, that they are consistent with log-normal for each individual flare class. This contradicts previous studies that have claimed that the distribution of flare durations is a power-law (*e.g.* Christe et al 2008), and importantly shows that the duration of the flare depends on what wavelength one observes the flare in.

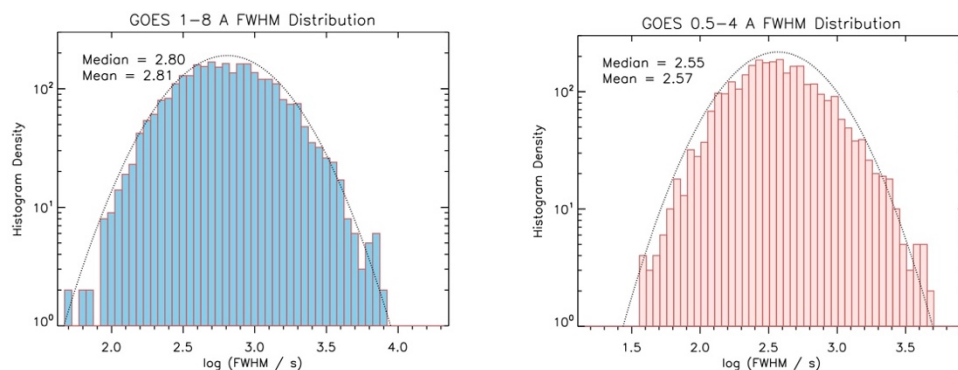


Fig. 2 — The distribution of flare durations, measured as FWHM in the two GOES passbands: 0.1–0.8 nm (left) and 0.05–0.4 nm (right). The distributions are consistent with log-normal, with median values of around 11 and 6 minutes, respectively.

Importantly, the duration of solar flares is not related to the size of the flare: there is no correlation between the flare class and the flare duration. We show this in Figure 3, and also show that there is no correlation between the total energy release and the duration. While we do not show it here, the temperature, EM, and reconnection flux are also not correlated with flare duration. This raises an important question: what causes the flare duration? Why is it unrelated to the size or energy release

of the flare? The only known correlation is with the separation of the two ribbons – roughly the separation of the footpoints of the longest loops in the flares (Toriumi et al 2017; Reep and Toriumi 2017). It is critical, however, to understand this duration, and requires accurate modeling, which is one motivation for development of the model described in the following sections.

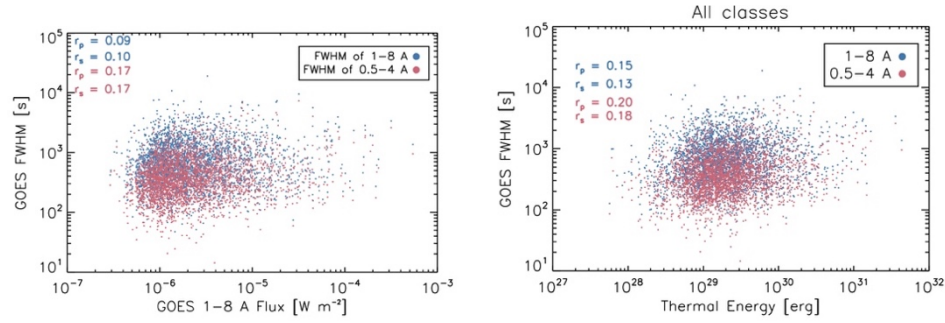


Fig. 3 — The absence of correlation between flare duration and class (left) and flare duration and total energy release (right). It is unknown why these quantities are not related, as might be expected.

3. EFFICIENT MODELING OF THE SOLAR CHROMOSPHERE IN HYDRODYNAMIC SIMULATIONS

Modeling the solar chromosphere accurately is crucial to understand the transport of energy through the different layers of the solar atmosphere. The chromosphere is optically thick at many wavelengths, necessitating solutions of the radiative transfer equation to accurately determine ionization fractions of different elements. Importantly, the ionization fraction of hydrogen, the dominant element in the plasma, is not characterized by local thermodynamic equilibrium (LTE) due to the non-negligible absorption and scattering of photons in this layer of the plasma. Therefore, in order to determine the ionization fraction, the following continuity equation must be solved:

$$\frac{\partial n_i}{\partial t} + \frac{\partial}{\partial s}(n_i v) = \sum_{j \neq i} n_j P_{ji} - n_i \sum_{j \neq i} P_{ij}$$

where n_i is the fractional level population of level i , v is the bulk flow velocity, P_{ij} is the total rate coefficient at which atoms transition from level i to j . This equation is solved simultaneously for a six-level hydrogen atom (that is, the first five states characterized by the principal quantum number n and the ionized state). This equation is closed by the requirement that the fractional levels must sum to 1. The rate coefficients P_{ij} are the sum of collisional and radiative rates:

$$P_{ij} = C_{ij} + R_{ij}$$

The collisional rate coefficients are taken from tables of atomic databases. The radiative rate coefficients, however, must be calculated based on the local plasma conditions, which is characteristic of non-LTE (NLTE) plasma. In order to accurately calculate the radiative rate coefficients, one needs to know the radiation field, which in turn requires accurate knowledge of the densities, and is a cyclical problem. The equations must therefore be solved iteratively, and we follow a prescription for the radiation field that was derived by Sollum (1999) as well as Leenaarts & Wedemeyer-Böhm (2006), based on a more detailed radiative transfer calculation. The calculation makes three assumptions to simplify the calculation: that the atmosphere is in LTE below a certain height, deep in the chromosphere; that the Lyman transitions are in detailed balance in the

chromosphere (see Carlsson & Stein 2002), which means that they are collisionally dominated; and that the radiation field can be characterized by a local brightness temperature. This prescription then allows for the iterative calculation of the radiative rate coefficients, and therefore the level populations and ionization fraction of hydrogen at various levels in the solar chromosphere (detailed in Reep et al. 2019a).

These methods have been implemented in the HYDrodynamics and RADiation code (HYDRAD, Bradshaw & Mason 2003; Bradshaw & Cargill 2013), which solves the equations that describe the conservation of mass, momentum, and energy of plasma constrained to a magnetic flux tube. This code has been extensively tested and used in a large number of studies regarding solar coronal heating, solar flares, and the solar wind. It includes the effects of thermal conduction, radiative losses calculated with the CHIANTI atomic database (Dere et al. 2019), cross-sectional area expansion, non-equilibrium ionization (Bradshaw & Raymond 2013), and electron beam heating (Reep et al. 2013).

3.1 Hydrodynamic Simulations

To test the method, we run hydrodynamic simulations of flaring loops heated by an electron beam. We use heating parameters derived from a combination of RHESSI and IRIS data (Warren et al 2016) for a small flare that occurred on November 19, 2014 at 14:14 UT. The flare produced significant brightenings in Si IV, C II, O I, and Mg II spectral lines observed by IRIS, as well as hard X-ray bremsstrahlung observed by RHESSI. The flare was also observed by Hinode/EIS, which provided density constraints using Fe XIV lines, SDO/AIA and Hinode/XRT which provided an EM distribution. In a previous paper, we had studied the flare with multithreaded modeling (Reep et al 2016), and found it to be incapable of reproducing the C II, O I, or Mg II emission. This primarily stems from these lines either not being optically thin or not in equilibrium.

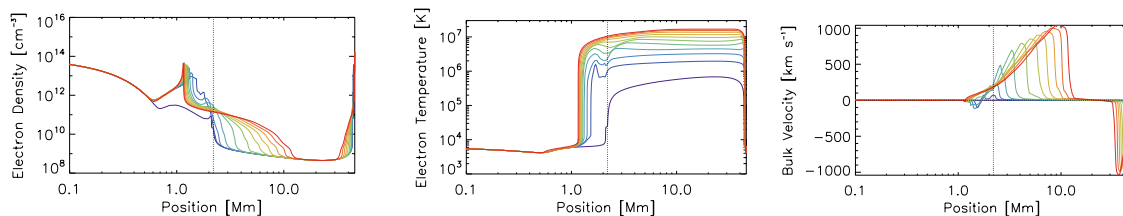


Fig. 4 — The evolution of electron density (left), temperature (center), and bulk velocity (right) in a hydrodynamic simulation of a flaring loop. The colors, from blue to red, show the change at a 1 second cadence.

In Figure 4, we show the typical evolution of a hydrodynamic simulation of a flaring loop subjected to heating by a strong electron beam. At left, the evolution of the electron density, which increases rapidly in the chromosphere as the heating and collisions with non-thermal electrons quickly ionize the hydrogen there. The temperature rises sharply in the corona to temperatures of around 20 MK, typical of the plasma that produces the sharp brightening of soft X-ray emission seen in solar flares. Finally, the heating of the chromosphere drives a sharp pressure expansion, leading to evaporative up-flows of plasma into the corona in excess of $1,000 \text{ km s}^{-1}$.

Figure 5 shows the evolution of the hydrogen level populations and ionization fraction for the same simulation. As the plasma is heated, the ionization fraction sharply rises towards 1 in the upper chromosphere and corona. The level populations above ground state also increases by a few orders of magnitude due to the collisional excitation of hydrogen from the non-thermal electrons which precipitate down the corona. The levels behave reasonably well compared to simulations that solve the full radiative transfer equation (compare, e.g. Allred et al. 2015 which uses the RADYN code, but it is much more computationally demanding).

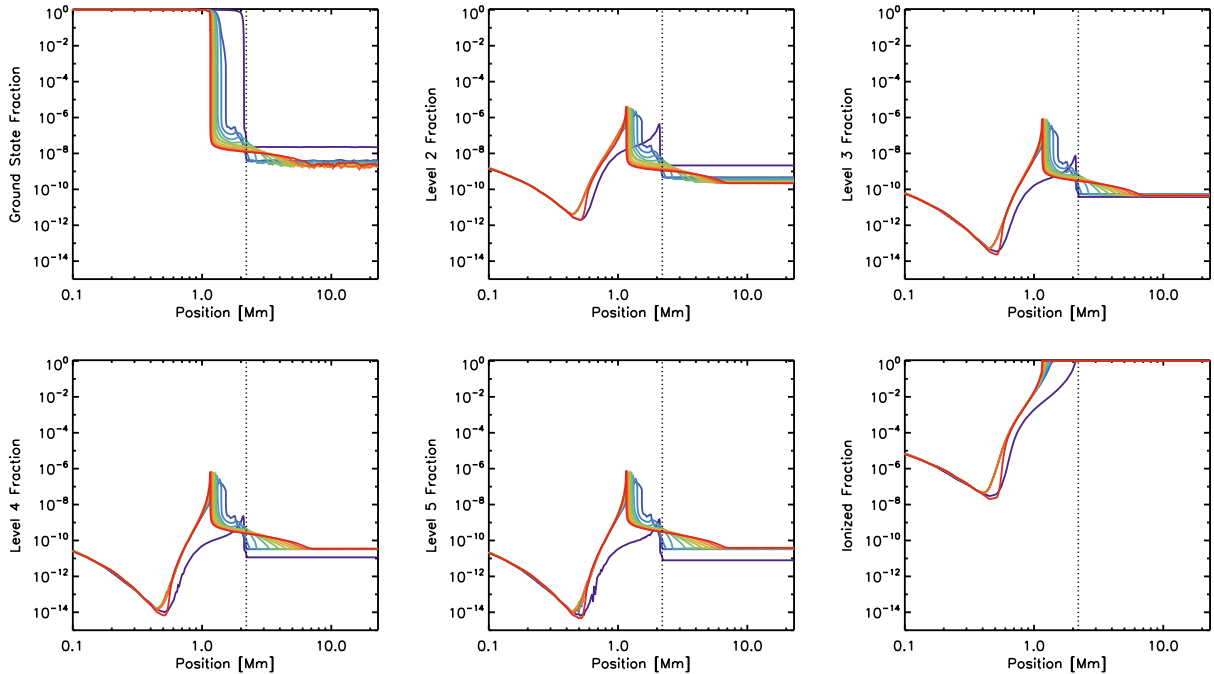


Fig. 5 — The evolution of the level populations of hydrogen for principle quantum number $n = 1$ through 5, as well as the ionized fraction of hydrogen at various heights. This is from the same simulation as in Figure 4.

3.2 Multithreaded Synthetic Light Curves

To test this model, we must compare with observations of flaring plasma. In a previous study by Warren et al. (2016), it was found in a small flare observed with IRIS that some spectral lines (Si IV 1402.7 and C II 1334.5) were red-shifted for the duration of a flare, implying that chromospheric condensation lasted for that long. This contradicts a long-standing result from hydrodynamic simulations of a flare that found that chromospheric condensations last around a minute, regardless of the total heating rate, duration, or other properties (Fisher 1989). A previous study found that these red-shifts could be explained with a succession of flaring loops *rooted within the same pixel* being energized in succession, which we term a multithreaded simulation (Reep et al. 2016). While that study was able to reproduce the observed properties of the Si IV emission, it failed to explain the C II emission (which had a strong stationary component) as well as O I 1334.5, which was observed to be completely stationary. It also was unable to address the slow decay of red-shifts observed in the Mg II 2796 line. One possible explanation for its failure was the lack of proper chromospheric modeling, in particular, that it did not address the optical thickness of the lines.

We therefore construct multithreaded light curves that properly treat the radiative transfer. We use the post-processing RH1.5D code (Pereira & Uitenbroek 2015), which solves the radiative transfer equations for a plane-parallel atmosphere. We then randomly select a number of hydrodynamic simulations, with varying heating rates, to construct multithreaded light curves using the output from RH. Finally, we fold the emission through the detector response appropriate to the spectrometer on the IRIS satellite so that we can compare directly to the observed quantities.

In Figure 6, we show three such examples. Each plot shows the synthetic light curves (top) and Doppler velocities (bottom) for C II 1334 (solid blue), O I 1355 (dashed pink), and Mg II 2796 (dotted green) constructed with a large number of threads N , using a power-law distribution of energies. From left to right, 60 threads spaced 10 seconds apart, 120 threads spaced 5 seconds apart,

and 600 threads spaced 1 second apart. In each case, the intensities of the light curves vary, the shapes of the Doppler shifts vary, and the smoothness of the curves vary. We find that the intensities are comparable to the observations (Warren et al 2016), though the oxygen line is too bright, while the Doppler shifts in all lines are roughly consistent with observations. The Mg II line looks most consistent with the right-hand plot, that is, with an extremely large number of threads, though the brightness of O I is too large.

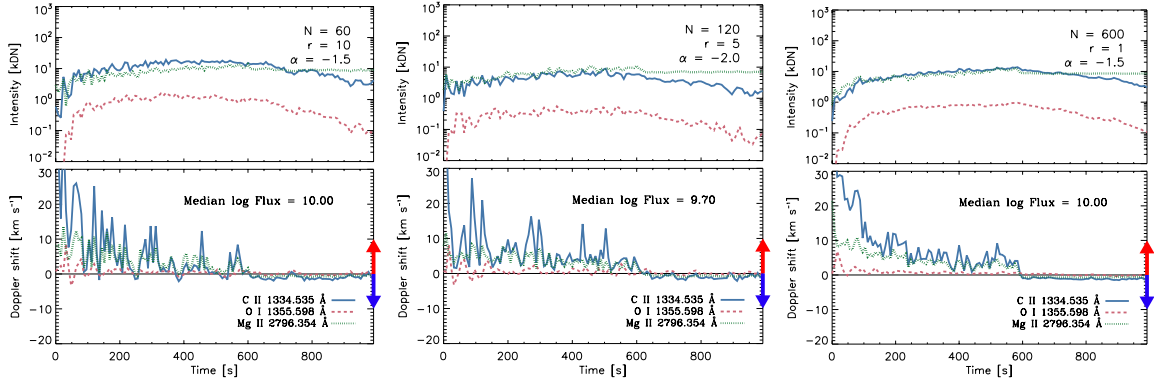


Fig. 6 — Multithreaded synthetic light curves and Doppler velocities for three spectral lines formed in the chromosphere, of varying optical thickness.

4. CONSTRUCTING A GLOBAL MODEL OF A SOLAR FLARE

With a proper chromospheric model in place, we now turn our focus towards constructing a global model of a flare, that can reproduce both its large-scale features (such as the GOES light curves) as well as the small-scale (*e.g.* spectral line shapes). To do this, we combine results from two previous studies that predict both the geometry of a solar flare and the heating rate as a function of time.

Warren (2006) derived a method to calculate the volume and heating rate of a succession of loops that can be used to reconstruct the GOES light curves extremely closely. In order to understand how this works, we note that the ratio of the two GOES channels scales directly with the temperature of the emitting plasma. For example, a 20 MK plasma produces much brighter emission in the high energy channel than a 10 MK plasma, so that ratio of the high energy channel to the low energy channel increases. This can be inverted to give an estimate of the plasma at a given time. Secondly, the strength of the emission in the two channels scales directly with the EM, which itself is proportional to the volume of the emitting region. Therefore, the ratio of the GOES channels along with their magnitude can be inverted to estimate both the volume and heating rate as a function of time for an observed solar flare, which can then be used as inputs. The equations are found to be:

$$V = \left(\frac{F_{1-8 \text{ \AA}}}{C} \right)^{9/2} \left(\frac{D}{F_{0.5-4 \text{ \AA}}} \right)^{7/2} L^2$$

$$E = \left(\frac{F_{1-8 \text{ \AA}}}{C} \right)^{5/2} \left(\frac{D}{F_{0.5-4 \text{ \AA}}} \right)^{3/2} L$$

where E is the heating rate, L is the loop length, and V the volume of the emitting region. In Warren (2006), the loop length L was assumed to be fixed.

In general, however, the lengths of the succession of energized loops will increase with time during a flare. In Reep & Toriumi (2017), for example, an increasing loop length was used to explain the observation that the FWHM of the GOES light curves was related to the separation of the flare ribbons. In order to model a realistic flare, we therefore need a realistic model for the loop lengths. We parameterize this in terms of the ribbon separation, which can be converted to lengths through simple geometry. We assume that the ribbons spread apart from some minimum distance to some maximum distance over the rising time of the GOES light curves. We empirically fit a hyperbolic tangent function to this separation:

$$d(t) = \frac{d_{\max} - d_{\min}}{2} \tanh\left(\frac{\omega(t - t_p)}{\tau_{\text{rise}}}\right) + \frac{d_{\max} + d_{\min}}{2}$$

which gives a simple (and differentiable) functional form for loop lengths as a function of time. This functional form is shown in Figure 7 at left, alongside an example observation from Hinterreiter et al. (2018), showing that it approximates the observed geometry well.

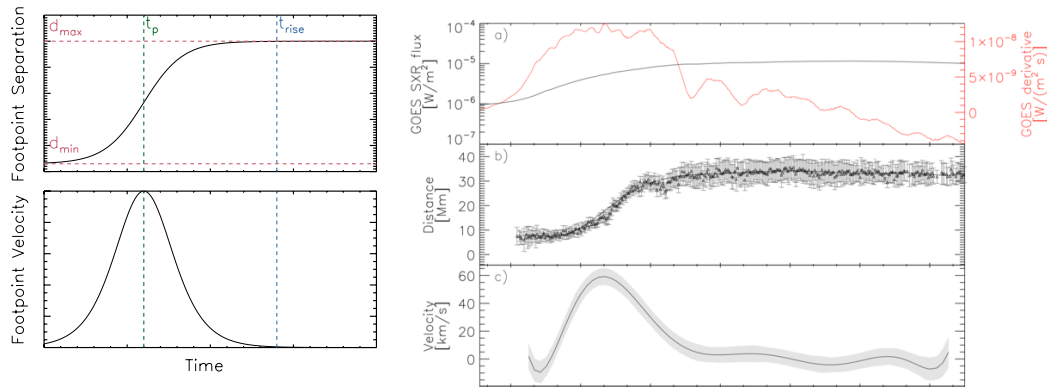


Fig. 7 — Model ribbon separation and velocity (left) compared to an observation of those same quantities (right), taken from Hinterreiter et al. (2018).

We then can use this combination of heating rates, volumes, and loop lengths to reconstruct the GOES light curves for any given flare with a succession of hydrodynamic simulations. With these simulations, we first validate the model by testing that it can reproduce other spectral emission and light curves, and then the model can be used for predictions of flare irradiance. The model can similarly be extrapolated to larger, unobserved flares to predict the impact on Earth.

4.1 Global Flaring Model – 2016 July 23 M5.0 Flare

We focus on the M5.0 flare which occurred on 2016 July 23 at around 01:45 UT. This flare was observed by GOES, SDO/AIA, as well as a soft X-ray spectrometer on board a cube-sat mission named MinXSS (Woods et al. 2017). The MinXSS spectra, in particular, offer high resolution spectra which can be contrasted with the model and test the parameters of the flare.

In Figure 8, we show the reconstruction of the two GOES channels. The heating rates and volumes have been derived from the observed light curves (green), and then a series of hydrodynamic simulations have been run to reproduce the light curves (each blue dashed line), which are then summed together to create a composite, synthetic light curve (solid blue). The hydrodynamic simulations use the derived heating rates, volumes, and loop lengths as described above. The observed and synthetic light curves are in close agreement, which is essentially by construction. The bottom plots show the ratio of the simulated to observed light curves, which are approximately

1 during the course of the flare in both channels, with some noise at the beginning and end of the flare when the background noise is comparable to the signal.

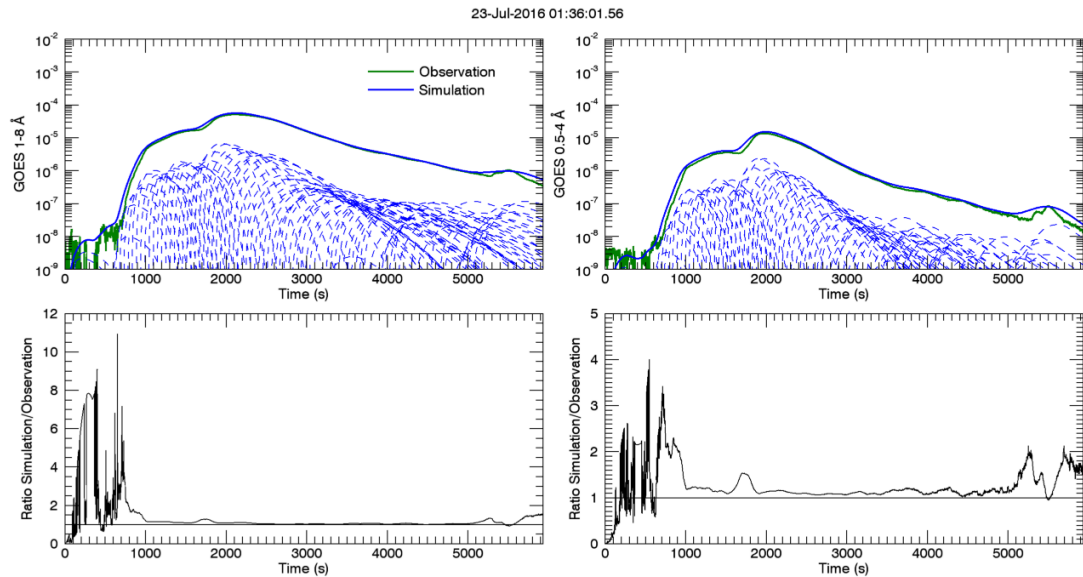


Fig. 8 — The construction of the global model. The heating rates and volumes are used to reconstruct the GOES light curves in both channels. The top shows the comparison between synthetic and observed, while the bottom shows their ratio.

Using this series of simulations, we then similarly produce light curves for 6 AIA channels, which form in lower temperature plasma than the GOES light curves. We also calculate the light curves and spectra in the soft X-ray range for comparison with that observed by MinXSS. In this way, we directly validate that the model is capable of faithfully reproducing other passbands besides what is observed by GOES. This means that if only GOES data were available, that we could still reproduce other light curves and spectra with the model.

In Figure 9, we show this comparison. At left, we show the six AIA channels (131, 94, 335, 211, 193, and 171), where the dots are the observed values and the solid lines are the synthetic light curves. We find good agreement in the hotter channels (131, 94, 335), while the cooler channels start to diverge in the late phase of the flare. On the right-hand side, we show a sample spectrum from MinXSS, where red shows the model spectrum and black the observed one. Here, we again find good agreement, particularly at energies greater than 2 keV, while there is some disagreement below that energy, due to a combination of the background and because the instrumental effective area decreases at low energies. The Fe XXV spectral line that forms around 6.7 keV, additionally, can be used to fit the elemental abundance of iron for the model.

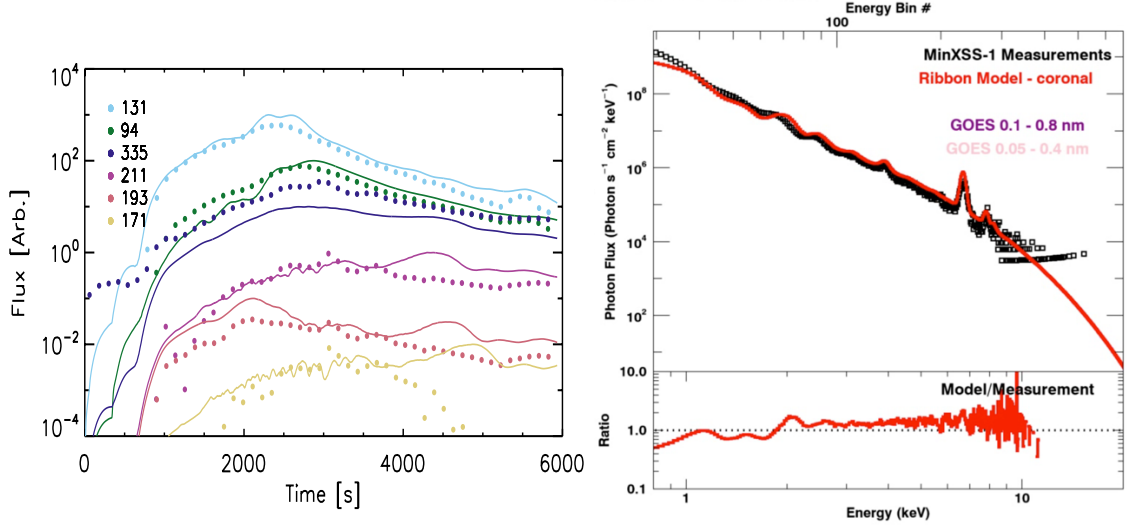


Fig. 9 — Comparison of observations and synthetic light curves in six AIA channels (left) as well as soft X-ray spectra observed by MinXSS (right).

4.2 Extrapolating the Global Flare Model

In order to make predictions about the irradiance of super-flares or flares of comparable size to the Carrington event (Carrington 1859), we need to understand how to scale both the volume and heating rate into unobserved ranges. In other words, the largest solar flares that have been observed by GOES are still significantly smaller than the Carrington event that was observed in 1859, which means that we do not have any significant data to determine what such an event should look like. Therefore, we plan to extrapolate this global flaring model.

In order to increase the GOES emission, we can scale it by either increasing the heating rate or the volume of the emitting region. In general, it is not clear whether scaling one or both of these would produce a more realistic model. We therefore have tried permutations where we scale each in different proportions. That is, we scale the total energy by a factor φ , and let the volume V and heating rate H of each thread i increase proportionally:

$$V_i \rightarrow \varphi^\alpha V_i$$

$$H_i \rightarrow \varphi^{1-\alpha} H_i$$

where we test different permutations by varying the parameter α . $\alpha = 0$ corresponds to linearly increasing the heating rate for a fixed volume, while $\alpha = 1$ corresponds to linearly increasing the volume for a fixed heating rate.

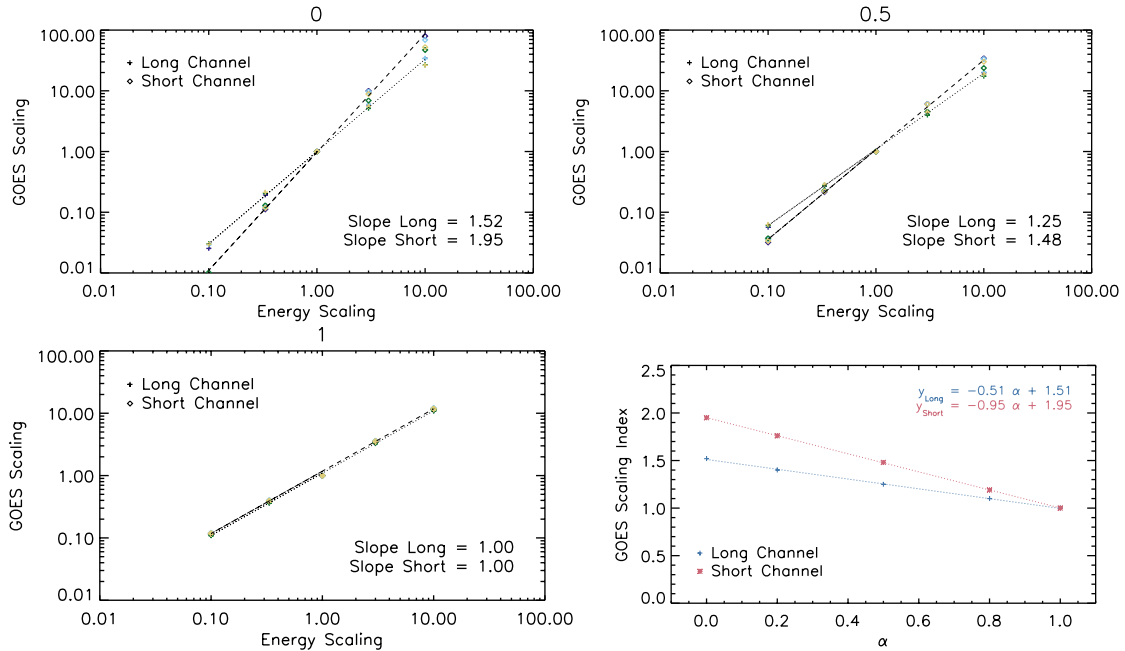


Fig. 10 — Extrapolations of the volume and heating rate for a small set of flares. We vary the parameter α and test how it affects the scaling laws (see text).

In Figure 10, we show the results of a numerical experiment to determine how the two GOES channels are impacted by varying the parameter α for a small set of flares (including the flare described in Section 4.1). The first three plots show how each flare scales for a given value of α (0, 0.5, 1, from top left). When $\alpha = 0$, the heating rate increases in a fixed volume, so the temperatures rise rapidly and the high energy channel increases rapidly. When $\alpha = 1$, the volume increases for a fixed heating rate, which means that both GOES channels scale linearly. Finally, the bottom right plot shows how the extrapolation changes for a few values of α . In general, we find that the two channels scale differently with the total energy input, which can be checked against observations.

How do real flares compare and what values should we use to extrapolate to superflares? To answer this, we return to the study presented in Section 2. In Figure 11, we show how the thermal energy scales with GOES class (left) and how the thermal energy scales with the ribbon area or similarly volume (right) for flares with energy above 10^{29} erg (where the signal-to-noise is good). The scaling of the GOES emission in each channel with the thermal energy is consistent with a value of α of around 0.8, while the scaling of the volume finds a value around 0.6. We plan to use these scalings in future work to predict spectra for Carrington-like events, and calculate the irradiance variation from them.

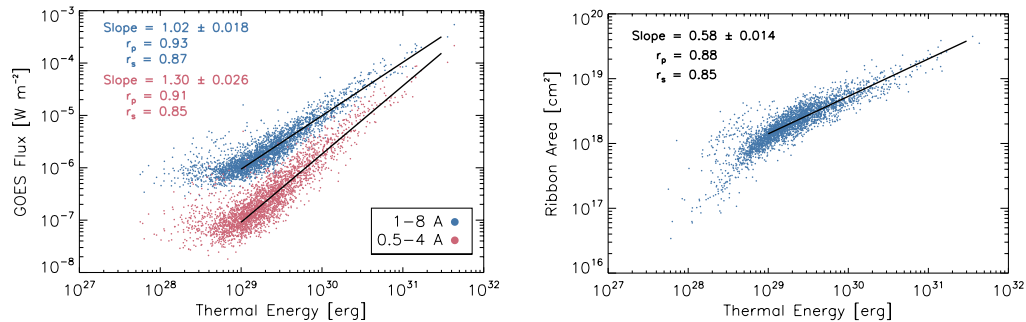


Fig. 11 — Observations of how the GOES class scales with the thermal energy (left) and the ribbon area or volume scales with the thermal energy (right) scale in a set of solar flares, from the data set presented in Section 2.

5. CONCLUSIONS

We have developed a global model of solar flares that can be used to predict irradiance variations due to events of any different size or duration, with any given set of properties. This irradiance prediction will be tied to the General Circulation Models of the ionosphere in on-going work, which will then be used to predict the impact upon radio communications. Furthermore, the model is being developed to make predictions of the parameters and impact upon Earth for extreme events like the Carrington flare of 1859, which have not been observed on the Sun with modern instrumentation.

In Section 2, we presented observations of solar flares that combined statistics taken with data from NOAA’s GOES satellites as well as NASA’s SDO satellite. It was found that the size or class of a solar flare scales with many basic parameters: temperature, emission measure (or density), volume or ribbon area, and magnetic flux. The duration of these flares, described by a log-normal distribution, however, is not correlated with any of these basic properties. The only correlation is with the separation of the two ribbons.

In Section 3, we developed a model of the solar chromosphere that is important to calculating the dynamics and radiative output of solar flares from hydrodynamic simulations. We employ a method that approximates the radiation field, which can then be used to calculate the radiative excitation, ionization, and recombination rates and solve for the hydrogen level populations and ionization fraction at all heights of the solar atmosphere. This allows us to accurately calculate the electron density, which is crucial for determining spectral emissions. We then verified this model by comparing hydrodynamic simulations and the post-processing radiative transfer calculations with observations by NASA’s IRIS satellite. The method works well to approximate the full radiative transfer calculation, and can therefore be used in hydrodynamic simulations of flares.

Finally, in Section 4, we have presented a method to construct a global model of a solar flare that accounts for the full arcade of many flaring loops being energized with time. It self-consistently calculates the time-varying heating rate, volume, and loop lengths to give a model that will reproduce the GOES light curves. We have validated the model by comparing to other observed quantities such as the SDO/AIA light curves in six emission bands cooler than GOES, as well as spectrally-resolved observations of soft X-ray spectra observed with the MinXSS cube-sat. The model can reproduce these quantities with good agreement, while simultaneously allowing us to constrain some basic parameters of the flare. Finally, we have calculated a method that allows us to extrapolate to large flares by increasing the volume and heating rates in a way that is consistent with observed scalings.

In future and on-going work, we will tie this unified model with models of the ionosphere-thermosphere-mesosphere system. We will provide high resolution and high cadence spectra

ranging from the X-rays through the optical band to Global Circulation Models. These GCM models can then calculate the impact of flares of varying sizes and durations upon the ionosphere, and calculate how radio wave communications are impacted by large flares.

Importantly, these will help us to understand the causes of variability in the solar irradiance and produce synthetic spectra that can determine the impact on HF and VHF radio systems. This work has improved the modeling and prediction of the solar irradiance, which is critical for Navy communications and HF radar.

ACKNOWLEDGEMENTS

This work is the subject of two published papers that appeared in the *Astrophysical Journal* [Reep et al. 2019, #19; Reep & Knizhnik 2019, #21] and one in preparation for submission to that same journal. The co-authors include Harry P. Warren, Nicholas A. Crump, and Kalman J. Knizhnik, of NRL (Code 7680) as well as Stephen J. Bradshaw of Rice University.

REFERENCES

1. Allred, Kowalski, & Carlsson, 2015. "A Unified Computational Model for Solar and Stellar Flares." *The Astrophysical Journal*, Vol. 809, 104. <https://doi.org/10.1088/0004-637X/809/1/104>
2. Bradshaw & Cargill, 2013. "The Influence of Numerical Resolution on Coronal Density in Hydrodynamic Models of Impulsive Heating." *The Astrophysical Journal*, Vol. 770, 12. <https://doi.org/10.1088/0004-637X/770/1/12>
3. Bradshaw & Mason, 2003. "A self-consistent treatment of radiation in coronal loop modelling." *Astronomy & Astrophysics*, Vol. 401, 699. <https://doi.org/10.1051/0004-6361:20030089>
4. Bradshaw & Raymond, 2013. "Collisional and Radiative Processes in Optically Thin Plasmas." *Space Science Reviews*, Vol. 178, 271. <https://doi.org/10.1007/s11214-013-9970-0>
5. Cargill and Priest, 1983. "The Heating of Postflare Loops." *The Astrophysical Journal*, Vol. 266, 383. <https://doi.org/10.1086/160786>
6. Carlsson and Stein, 2002. "Dynamic Hydrogen Ionization." *The Astrophysical Journal*, Vol. 572, 626. <https://doi.org/10.1086/340293>
7. Carrington, 1859. "Description of a Singular Appearance seen in the Sun on September 1, 1859." *Monthly Notices of the Royal Astronomical Society*, Vol. 20, 13. <https://doi.org/10.1093/mnras/20.1.13>
8. Christe, Hannah, Krucker, et al. 2008. "RHESSI Microflare Statistics. I. Flare-Finding and Frequency Distributions." *The Astrophysical Journal*, Vol. 677, 1385. <https://doi.org/10.1086/529011>
9. Dere, Del Zanna, Young, et al., 2019. "CHIANTI – An Atomic Database for Emission Lines. XV. Version 9, Improvements for the X-ray Satellite Lines." *The Astrophysical Journal Supplement Series*, Vol. 241, 22. <https://doi.org/10.3847/1538-4365/ab05cf>
10. Fisher, 1989. "Dynamics of Flare-driven Chromospheric Condensations." *The Astrophysical Journal*, Vol. 346, 1019. <https://doi.org/10.1086/168084>
11. Fletcher, Dennis, Hudson, et al., 2011. "An Observational Overview of Solar Flares." *Space Science Reviews*, Vol. 159, 19. <https://doi.org/10.1007/s11214-010-9701-8>
12. Hinterreiter, Veronig, Thalmann, et al., 2018. "Statistical Properties of Ribbon Evolution and Reconnection Electric Fields in Eruptive and Confined Flares." *Solar Physics*, Vol. 293, 38. <https://doi.org/10.1007/s11207-018-1253-1>
13. Hirayama, 1974. "Theoretical Model of Flares and Prominences. I: Evaporating Flare Model." *Solar Physics*, Vol. 34, 323. <https://doi.org/10.1007/BF00153671>
14. Holman, Aschwanden, Aurass, et al., 2011. "Implications of X-ray Observations for Electron Acceleration and Propagation in Solar Flares." *Space Science Reviews*, Vol. 159, 107. <https://doi.org/10.1007/s11214-010-9680-9>
15. Hudson, 1991. "Solar Flares, Microflares, Nanoflares, and Coronal Heating." *Solar Physics*, Vol. 133, 357. <https://doi.org/10.1007/BF00149894>
16. Kazachenko, Lynch, Welsch, and Sun, 2017. "A Database of Flare Ribbon Properties from the Solar Dynamics Observatory. I. Reconnection Flux." *The Astrophysical Journal*, Vol. 845, 49. <https://doi.org/10.3847/1538-4357/aa7ed6>
17. Leenaarts & Wedemeyer-Böhm, 2006. "Time-dependent Hydrogen Ionisation in 3D simulations of the Solar Chromosphere. Methods and First Results." *Astronomy & Astrophysics*, Vol. 460, 301. <https://doi.org/10.1051/0004-6361:20066123>
18. Pereira & Uitenbroek, 2015. "RH1.5D: a massively parallel code for multi-level radiative transfer with partial frequency redistribution and Zeeman polarisation." *Astronomy & Astrophysics*, Vol. 574, 3. <https://doi.org/10.1051/0004-6361/201424785>

19. Reep, Bradshaw, Crump, and Warren, 2019a. “Efficient Calculation of Non-local Thermodynamic Equilibrium Effects in Multithreaded Hydrodynamic Simulations of Solar Flares.” *The Astrophysical Journal*, Vol. 871, 18. <https://doi.org/10.3847/1538-4357/aaf580>
20. Reep, Bradshaw, and McAteer, 2013. “On the Sensitivity of the GOES Flare Classification to Properties of the Electron Beam in the Thick-Target Model.” *The Astrophysical Journal*, Vol. 778, 76. <https://doi.org/10.1088/0004-637X/778/1/76>
21. Reep & Knizhnik, 2019. “What Determines the X-ray Intensity and Duration of a Solar Flare?” *The Astrophysical Journal*, Vol. 874, 157. <https://doi.org/10.3847/1538-4357/ab0ae7>
22. Reep & Toriumi, 2017. “The Direct Relation between the Duration of Magnetic Reconnection and the Evolution of GOES Light Curves in Solar Flares.” *The Astrophysical Journal*, Vol. 851, 4. <https://doi.org/10.3847/1538-4357/aa96fe>
23. Reep, Warren, Crump, and Simões, 2016. “Transition Region and Chromospheric Signatures of Impulsive Heating Events. II. Modeling.” *The Astrophysical Journal*, Vol. 827, 145. <https://doi.org/10.3847/0004-637X/827/2/145>
24. Reep, Warren, Moore, Suarez, and Hayes, 2019b. “Simulating Soft X-Ray Irradiances Using Multithreaded Models of Flare Arcades.” In preparation for submission to the *Astrophysical Journal*.
25. Sheeley, Warren, and Wang, 2004. “The Origin of Postflare Loops.” *The Astrophysical Journal*, Vol. 616, 1224. <https://doi.org/10.1086/425126>
26. Sollum, 1999. “Hydrogen Ionization in the Solar Atmosphere: Exact and Simplified Treatments.” Master’s Thesis, University of Oslo.
27. Tarr, 2017. “On Excited Frequencies for Alfvén Waves in a Coronal Arcade.” *The Astrophysical Journal*, Vol. 847, 1. <https://doi.org/10.3847/1538-4357/aa880a>
28. Toriumi, Schrijver, Harra, et al., 2017. “Magnetic Properties of Solar Active Regions That Govern Large Solar Flares and Eruptions.” *The Astrophysical Journal*, Vol. 834, 56. <https://doi.org/10.3847/1538-4357/834/1/56>
29. Warren, 2006. “Multithread Hydrodynamic Modeling of a Solar Flare.” *The Astrophysical Journal*, Vol. 637, 522. <https://doi.org/10.1086/497904>
30. Warren, Reep, Crump, & Simões, 2016. “Transition Region and Chromospheric Signatures of Impulsive Heating Events. I. Observations.” *The Astrophysical Journal*, Vol. 829, 35. <https://doi.org/10.3847/0004-637X/829/1/35>
31. Woods, Caspi, Chamberlin, et al., 2017. “New Solar Irradiance Measurements from the Miniature X-Ray Solar Spectrometer CubeSat.” *The Astrophysical Journal*, Vol. 835, 122. <https://doi.org/10.3847/1538-4357/835/2/122>